Diabetes-induced myelin abnormalities are associated with an altered lipid pattern: protective effects of LXR activation[S]

Gaia Cermenati,[1,*] Federico Abbiati,[1,*] Solei Cermenati,[†] Elisabetta Brioschi,[*] Alessandro Volonterio,[**] Guido Cavaletti,[††] Enrique Saez,[§§] Emma De Fabiani,[*] Maurizio Crestani,[*] Luis M. Garcia-Segura,[***] Roberto C. Melcangi,[§] Donatella Caruso,[*] and Nico Mitro[*]

Department of Pharmacological Sciences,* Department of Biomolecular Sciences and Biotechnologies,[†] and Department of Endocrinology, Pathophysiology and Applied Biology,[§] Center of Excellence on Neurodegenerative Diseases, Università degli Studi di Milano, Milano, Italy; Department of Chemistry,** Material and Chemical Engineering "Giulio Natta," Politecnico di Milano, Milano, Italy; Department of Neurosciences and Biomedical Technologies,[††] Università degli Studi di Milano "Bicocca," Milano, Italy; Department of Chemical Physiology and Skaggs Institute for Chemical Biology,[§§] The Scripps Research Institute, La Jolla, CA; and Instituto Cajal,*** C.S.I.C., Madrid, Spain.

Abstract Diabetic peripheral neuropathy (DPN) is characterized by myelin abnormalities; however, the molecular mechanisms underlying such deficits remain obscure. To uncover the effects of diabetes on myelin alterations, we have analyzed myelin composition. In a streptozotocin-treated rat model of diabetic neuropathy, analysis of sciatic nerve myelin lipids revealed that diabetes alters myelin's phospholipid, FA, and cholesterol content in a pattern that can modify membrane fluidity. Reduced expression of relevant genes in the FA biosynthetic pathway and decreased levels of the transcriptionally active form of the lipogenic factor sterol-regulatory element binding factor-1c (SREBF-1c) were found in diabetic sciatic nerve. Expression of myelin's major protein, myelin protein zero (P0), was also suppressed by diabetes. In addition, we confirmed that diabetes induces sciatic nerve myelin abnormalities, primarily infoldings that have previously been associated with altered membrane fluidity. In a diabetic setting, synthetic activator of the nuclear receptor liver X receptor (LXR) increased SREBF-1c function and restored myelin lipid species and P0 expression levels to normal. These LXR-modulated improvements were associated with restored myelin structure in sciatic nerve and enhanced performance in functional tests such as thermal nociceptive threshold and nerve conduction velocity. These findings demonstrate an important role for the LXR-SREBF-1c axis in protection from diabetes-induced myelin abnormalities.—Cermenati, G., F. Abbiati, S. Cermenati, E. Brioschi, A. Volonterio, G. Cavaletti, E. Saez, E. De Fabiani, M. Crestani, L. M. Garcia-Segura, R. C. Melcangi, D. Caruso, and N. Mitro. **Diabetes-induced myelin abnormalities are associated with an altered lipid pattern: protective effects of LXR activation.** ***J. Lipid Res.*** **2012.** 53: **300–310.**

Supplementary key words diabetic neuropathy • liver X receptor • myelin composition • peripheral nerve • sterol-regulatory element binding factor-1c • fatty acid synthesis

Diabetic peripheral neuropathy (DPN) appears frequently in patients diagnosed with type 1 or type 2 diabetes (1–3). The extent of abnormalities is more pronounced if the hyperglycemia is not controlled properly (4, 5). DPN is associated with deleterious changes in peripheral nerves, such as myelin damage and decrease in nerve conduction velocity (4–9). Similar structural abnormalities and neurophysiological changes have been observed in the peripheral nerves of streptozotocin (STZ)-treated rats, an experimental model that captures many features of type 1 diabetes (10–12). As it is seen in diabetic subjects, STZ-treated rats show increased morphological alterations in the myelinated fibers of the sciatic nerve (13).

This work was supported by a Giovanni Armenise-Harvard Foundation Career Development Grant (NM).

Manuscript received 30 September 2011 and in revised form 5 December 2011.

Published, JLR Papers in Press, December 7, 2011
DOI 10.1194/jlr.M021188

Abbreviations: DPN, diabetic peripheral neuropathy; GSL, glycosphingolipid; IS, internal standard; LXR, liver X receptor; P0, myelin protein zero; PC, phosphatidyl choline; PE, phosphatidyl ethanolamine; PI, phosphatidyl inositol; PMP22, peripheral myelin protein 22; PS, phosphatidyl serine; SCD-1, stearoyl-CoA desaturase-1; SCD-2, stearoyl-CoA desaturase-2; SM, sphingomyelin; SREBF-1c, sterol-regulatory element binding factor-1c; STZ, streptozotocin; Sulf, sulphatides; TEM, transmission electron microscopy.

[1] G. Cermenati and F. Abbiati contributed equally to this work.

[2] To whom correspondence should be addressed.
e-mail: nico.mitro@unimi.it (N.M.); donatella.caruso@unimi.it (D.C.)

[S] The online version of this article (available at http://www.jlr.org) contains supplementary data in the form of four figures.

The myelin sheath is a multilayered membrane produced in the peripheral nervous system by differentiation of the plasmatic membrane of Schwann cells (14). The main role of this membrane is to allow efficient transmission of nerve impulses along the axons that it surrounds (15). A major biochemical characteristic that distinguishes myelin from other biological membranes is its high lipid-to-protein ratio: isolated myelin contains 70–80% lipids and 20–30% proteins. This high lipid content and the nature of the lipids present in the sheath provide the reduction of internodal capacitance required for saltatory propagation of the nervous influx (14). Myelin does not contain distinctive lipids; however, lipid components of myelin present a peculiar distribution when compared with those found in nonmyelin membranes (14, 16, 17). Cholesterol represents 20–30% of the lipid present in the peripheral nervous system (14), and its role in myelin is to stabilize and compact the membrane (18, 19). In contrast to lipids, myelin is characterized by the presence of proteins that are exclusively found there. In peripheral nerves, about 60% of myelin proteins are glycoproteins (which are less represented in the central nervous system), whereas 20–30% are basic proteins, and the rest belong to various protein classes (14, 16, 17).

Recently, it has been reported that in BB/Wor diabetic rats, type 1 diabetes reduces the expression of the lipogenic transcription factor sterol-regulatory element binding factor-1c (SREBF-1c) in Schwann cells (20). It has also been shown that the acute phase of myelin lipid synthesis is regulated by SREBF cleavage activating protein (SCAP), an activator of SREBFs (21). These observations suggest that lack of insulin and/or of transcriptionally active SREBF-1c in peripheral nerves leads to decreased lipogenesis. Diminished or abnormal FA synthesis may play an important role in altered myelin lipid and protein composition. Such changes in myelin could affect membrane fluidity and function, ultimately contributing to the pathogenesis of DPN (21, 22). In support of this notion, studies in animal models have revealed a protective effect of administration of FAs on DPN (23). However, the specific changes in myelin lipid and protein composition induced by diabetes, as well as the molecular mechanism responsible for these defects, remain to be identified. Detailed investigation of myelin's composition and elucidation of these mechanisms may suggest an approach to restoring defects in FA biosynthesis present in diabetic myelin and their role in myelin structure.

We have previously shown that treatment of STZ-treated rats with a synthetic liver X receptor (LXR) ligand promotes cholesterol utilization and increases neuroactive steroid levels in sciatic nerve, resulting in significant improvements in thermal nociceptive activity, nerve conduction velocity, and Na^+K^+-ATPase activity (24). The LXRs are ligand-activated nuclear receptors that control cholesterol and lipid metabolism. Both LXRα and LXRβ (NR1H3 and NR1H2) are expressed in sciatic nerve (24). Neuroactive steroid levels are decreased in peripheral nerves of STZ diabetic rats (25, 26), and treatments that restore their levels improve DPN and myelin function (13, 27, 28). In addition to their role in the regulation of cholesterol homeostasis, the LXRs also modulate FA metabolism. In fact, the LXRs directly regulate expression of the lipogenic transcription factor SREBF-1c, and of key enzymes involved in FA biosynthesis, such as fatty acid synthase (FAS) and stearoyl-CoA desaturase-1 (SCD-1) (29, 30). The ability of LXRs to modulate lipid levels prompted us to evaluate the potential of a synthetic LXR activator to reverse diabetes-induced lipid abnormalities in sciatic nerve myelin.

Here, we report that rats with DPN display an altered myelin lipid composition pattern, blunted expression of key genes in the FA biosynthetic pathway, and decreased levels of the active form of the lipogenic transcription factor SREBF-1c and the chief myelin protein zero (P0). These defects are associated with increased myelin infoldings in the sciatic nerve of diabetic rats. Activation of LXR with a synthetic ligand normalizes myelin's lipid profile, restores expression of genes involved in FA biosynthesis, reestablishes nuclear levels of SREBF-1c and absolute levels of P0, and corrects the major myelin abnormalities induced by diabetes in peripheral nerves. These changes are associated with improved performance in functional tests. Our findings suggest that activation of the LXR-SREBF-1c pathway may be useful to correct diabetes-associated peripheral nerve abnormalities.

MATERIALS AND METHODS

Animals

All experiments were conducted strictly following the regulations of European Community Directive 86/609/EEC (Official Journal L 358, 18/12/1986, pp. 0001–0028), and local regulations (e.g., Italian Legislative Decree n. 116, 27/01/1992) for the care and use of laboratory animals. Animal protocols were approved by the Institutional Review Committee. Diabetes was induced by a single intraperitoneal injection of STZ, 65 mg/kg (Sigma-Aldrich; Milano, Italy) in 0.09 M citrate buffer, pH 4.8, in 2-month-old male Sprague-Dawley rats (Crl:CD BR, Charles River; Lecco, Italy). Hyperglycemia was verified after 2 days, and rats with blood glucose concentrations >300 mg/dl were included in these studies. Two months after the induction of diabetes, animals were treated once a week with a subcutaneous injection of the synthetic LXR ligand GW3965 (i.e., four treatments in a month at 50 mg/kg) for a month. Nondiabetic and diabetic control rats were treated with vehicle. GW3965 was synthesized as previously described (24). Nondiabetic rats receiving GW3965 and their relative controls were treated with the same protocol described for STZ-diabetic rats.

Thermal nociceptive threshold and nerve conduction velocity

Neurophysiological studies were performed throughout the 3 months of diabetes to evaluate development of peripheral neuropathy and the effects of LXR activation as previously described (24). The tests were done in a temperature-controlled room adjacent to the animals' housing room and animals' vital parameters were monitored.

Myelin lipidomic analyses

Reagents. The internal standards (ISs) heneicosanoic acid (C21:0) and 5α-cholestane, and all other standards for FAs and cholesterol analyses were purchased from Sigma-Aldrich.

Phospholipid, FA, and cholesterol extraction methods. Myelin was purified from sciatic nerve of control, STZ, and STZ-treated with GW3965 rats as previously described (31). Internal standards were added to myelin samples, and lipid extraction was performed using the Folch method [chloroform-methanol (MeOH) 2:1, v/v]. Samples were left overnight at 4°C. Then the organic residue was divided in two fractions: one for the analysis of free cholesterol and phospholipids (fraction A, 60% of the total sample), and the other for analysis of total FAs and total cholesterol (fraction B, 40% of the total sample). Total FAs and cholesterol were obtained from samples by acid hydrolysis (32). Fraction B was resuspended in chloroform-MeOH 1:1, v/v. 1M HCl:MeOH (1:1, v/v) was added to the total lipid extract and shaken for 2 h. Then chloroform-water (1:1, v/v) was added, and the lower organic phase was collected, split, transferred into tubes and dried under nitrogen flow. The residue was resuspended in 1 ml of MeOH and split 60/40 for total FA and total cholesterol analysis, respectively.

Lipidomic profile by LC-MS/MS. The aliquot for FA quantification was suspended in MeOH, concentrated, and transferred into auto-sampler vials for LC-MS/MS analysis. Quantitative analysis was performed on the basis of calibration curves prepared and analyzed using standards. Electrospray ionization (ESI) experiments were performed using a linear ion trap-mass spectrometer equipped with a Surveyor liquid chromatography Pump Plus and a Surveyor Autosampler Plus. The LC mobile phases were water and MeOH/2-propanol (50:50, v/v). The gradient (flow rate 0.2 ml/min) was as follows: T_0: 100% A, T_5: 100% A, $T_{5.1}$: 50% A, T_{25}: 50% A, $T_{25.1}$: 100% A, T_{40}: 100% A. The Hypersil GOLD™ pentafluorophenyl column (100 mm × 2.1 mm, 3 μm) was maintained at 40°C. The injection volume was 20 μl, and the injector needle was washed with MeOH-water 1:1 (v/v). Peaks off the LC-MS/MS were evaluated using a Dell workstation by means of the software Excalibur, release 2.0 SR2. The mass spectrometer was operated in negative-ion mode with the ESI source using nitrogen as sheath, auxiliary, and sweeps gas, respectively. The mass spectrometer was operated in MS/MS mode using helium as a collision gas. The relative collision energy was set at 35% for all analyzed molecules. Principal component analysis was performed using Unscrambler, version 10.1 (Camo Software; Oslo, Norway).

Cholesterol quantification. Fractions for the quantitative analysis of free and total cholesterol, were first derivatized with a mixture of bis-trimethylsilyltrifluoroacetamide-pyridine (4:1 v/v) for 30 min at 60°C, and then injected into a gas chromatograph-mass spectrometer (GC-MS, Varian Saturn 2100). The MS was operated in the electron impact ionization mode. GC-MS analyses were performed as follows: 1 μl sample was injected in splitless mode (inlet was kept at 270°C with the helium flow at 1.0 ml/min) at the initial 180°C. The oven was first kept at 180°C for 1 min, ramped at 50°C/min to 240°C, then at 5°C/min to 300°C for 6 min. The ions used for the quantification of cholesterol were at *m/z* 368 for cholesterol and *m/z* 357 for 5α-cholestane, the IS. The selection of ions for selective ion monitoring analysis was based on mass spectra of pure standards, and the quantification was based on calibration curves freshly prepared using a fixed concentration of the IS, and different concentrations of cholesterol, in a range from 0 to 10 μg/μl. The amount of cholesteryl esters was calculated by subtracting the amount of free cholesterol from total cholesterol. Cholesteryl esters were evaluated to verify the myelin quality and purity.

Phospholipid analysis. ESI analysis of the major phospholipid classes was accomplished by utilization of either positive or negative ionization modes. Samples were directly infused for acquisition of MS/MS spectra. Changes between detected phospholipid families were calculated as percent of single phospholipid species normalized to total phospholipid analyzed.

Quantitative real-time PCR

RNA was prepared using the Nucleospin® RNA II kit (Macherey-Nagel; Milano, Italy). RNA was analyzed by TaqMan CFX384 RT-qPCR using the iScriptTM one-step RT-PCR kit for probes (Bio-Rad; Milano, Italy). Samples were arrayed in 384-well format in triplicate as multiplexed reactions of target gene with 36B4 as reference gene. Probe and primer sequences were purchased from Eurofins MWG-Operon (Milano, Italy) and are available on request.

Transfection and protein analysis

Expression constructs flag tagged for the mature forms of SREBF-1a, SREBF-1c, and SREBF-2 were a gift of Dr. T. Osborne (Addgene plasmid #26801, #26802, and #26807, respectively; Addgene, Cambridge, MA). Five micrograms of each SREBF expression construct and 5 μg of pcDNA3 (the backbone plasmid of the SREBFs) were transfected individually in Hek293T cells using FuGENE 6 (Promega; Milano, Italia) according to manufacturing instructions in 6-well tissue culture plates. Six hours after transfection, the cells were cultured in DMEM with 10% FBS, and 48 h later, total protein extracts were prepared using modified RIPA buffer [50 mM Tris-HCl (pH 7.4), 1% Nonidet P-40, 0.25% sodium deoxycholate, 150 mM NaCl, 1 mM EDTA, and protease inhibitor mixture (Roche; Monza, Italy)]. Western blotting was performed with a mouse monoclonal anti-SREBF-1 (Santa Cruz Biotechnology; Milano, Italy) at a dilution of 1:200, or a mouse polyclonal anti-Flag 1:1,000 (Sigma-Aldrich).

Sciatic nerves from three different animals per experimental group were lysed using modified RIPA buffer. Western blotting was performed with a mouse monoclonal anti-SREBF-1 (Santa Cruz Biotechnology) at a dilution of 1:200, a rabbit polyclonal anti-P0 (Sigma-Genosys; Milano, Italy) at a dilution of 1:500, or a rabbit polyclonal anti-peripheral myelin protein 22 (PMP22) (Inbios; Napoli, Italy) at a dilution of 1:5,000. As a loading control, membranes were probed with a mouse monoclonal anti-β-actin (Sigma-Aldrich) at a dilution of 1:1,000. All secondary antibodies were from Sigma-Aldrich. Quantification of protein levels was performed using Quantity One software (Bio-Rad). Analyses of protein levels were repeated at least three times with different sets of animals.

Immunofluorescence

To analyze protein expression of SREBF-1c, we incubated fixed slides with mouse monoclonal anti-SREBF-1 (Santa Cruz Biotechnology) at a dilution of 1:20 overnight at 4°C. Slides were then incubated with a goat anti-mouse Alexa Fluor 488 at a dilution of 1:500 (Invitrogen, Milano, Italy), and staining was completed using Hoechst 33258 (Invitrogen). Image acquisition was performed using a Leica TCS SP2 AOBS Spectral confocal scanner mounted on a Leica DM IRE2 inverted fluorescent microscope with the Leica LCS™ software. A 63× Leica oil objective and a 2× digital zoom were used for all observations. To compare different experimental conditions, fluorescence acquisitions were always performed with the same hardware settings (laser intensity, sampling, acquisition rate, pinhole, and photomultiplier settings). SREBF-1c localization was assessed by maximum projections (eight pictures per stack). Regions of interest are drawn to outline precisely the nuclei and the presence of SREBF-1c protein within the nuclei. SREBF-1c protein quantity in nuclei was calculated as mean amplitude and expressed as fluorescence intensity (arbitrary unit). Fluorescence intensity was measured off-line, using the stack profile module and analyzed by digital image

processing software (Leica LCS™ software; Milano, Italy). Nuclei were analyzed in at least three different fields of the same slide and from at least two different preparations for each experimental condition. For the colocalization quantification of SREBF-1c-containing nuclei, we counted positive nuclei in three different fields of the same slide and from at least three different preparations.

Morphometric analysis and transmission electron microscopy

Sciatic nerves were removed, cut in segments (1–2 mm length) and fixed by immersion in 1% paraformaldehyde and 1% glutaraldehyde in 0.1 M phosphate buffer, pH 7.4, for 24 h at 4°C. Tissue samples were washed in phosphate buffer, postfixed for 2 h in 1% buffered OsO_4, dehydrated, and embedded in araldite. Nerves were sectioned transversely using a Reichert Ultra-cut microtome. Semi-thin sections (0.5 μm) were stained with toluidine blue and analyzed by light microscopy. Thin sections were examined using a JEOL 1200 EXII electron microscope.

For morphometric analysis of myelinated fibers, areas of semithin sections, covering at least 25% of the total cross-sectional profile of the nerve, were chosen by systematic random sampling of squares (33, 34). The size of axons, the *g* ratio, the percentage of normal and abnormal fibers, the percentage of fibers with irregular shapes, with infoldings and with alteration in myelin compaction, were analyzed using a JEOL 1200 EXII electron microscope. The *g* ratio was calculated as the quotient between the axon size and the fiber size (35, 36). A minimum of 100 myelinated fibers were assessed from at least eight animals per group.

Statistical analyses

Statistical analyses were performed via one-way ANOVA followed by Tukey-Kramer posttest. All statistical analyses were performed with GraphPad PRISM version 5 (San Diego, CA).

RESULTS

DPN induces changes in myelin lipid composition, a pattern that is reversed by activation of LXR

Diabetes was induced in adult Sprague-Dawley rats by a single STZ injection. To explore the role of myelin lipids in the pathogenesis of DPN, and to evaluate whether LXR activation (through its ability to induce the master regulator of lipogenesis, SREBF-1c) could play a part, we compared age-matched nondiabetic and STZ-treated rats dosed with either vehicle or the synthetic LXR ligand GW3965 once a week for a month, starting two months after the induction of diabetes. Three months after the induction of diabetes, both groups of STZ-treated rats showed decreased body weight and increased glycemia relative to nondiabetic controls (**Table 1**). As previously demonstrated, diabetes affected functional parameters such as thermal nociceptive threshold and nerve conduction velocity, indicating that the animals developed peripheral neuropathy. LXR activation reversed these diabetes-induced peripheral nerve deficits (Table 1 and as reviewed in Ref. 24).

To test the hypothesis that diabetes induces an altered lipid composition profile in peripheral nerves, we performed detailed lipidomic analyses on sciatic nerve myelin purified from control, STZ, and STZ-GW3965-treated rats. The phospholipid profile of purified myelin revealed that diabetes primarily decreases the levels of glycosphingolipids

TABLE 1. Body weight, glycemia, thermal nociceptive threshold, and nerve conduction velocity of control and STZ rats treated with vehicle or GW3965

	Control	STZ	STZ+GW3965
Weight (g)	562.70 ± 47.21	272.13 ± 40.2[a]	285.20 ± 47.96[a]
Glycemia (mg/dl)	144.23 ± 23.35	608.65 ± 78.3[a]	555.61 ± 37.63[a]
Thermal nociceptive threshold (s)	8.15 ± 1.17	32.90 ± 3.65[a]	18.94 ± 2.10[b,c]
Nerve conduction velocity (m/s)	33.15 ± 1.27	22.23 ± 0.44[a]	27.62 ± 1.01[b,c]

Statistical analysis was performed by one-way ANOVA followed by Tukey-Kramer posttest. Data are expressed as mean ± SEM. n = 11 animals per group.

[a] $P < 0.001$ versus control rats.

[b] $P < 0.05$ versus control rats.

[c] $P < 0.05$ versus STZ-treated rats.

(GSLs), whereas phosphatidyl serine (PS) and phosphatidyl choline (PC) were mildly increased (**Fig. 1A**). Levels of phosphatidyl ethanolamine (PE), phosphatidyl inositol (PI), sphingomyelin (SM), and sulfatides (Sulf) were unchanged (Fig. 1A). We also detected a 60% decrease in sciatic nerve myelin cholesterol content (Fig. 1B). Remarkably, LXR activation in this diabetic setting restored the levels of all these lipids to those found in the nondiabetic control group (Fig. 1A, B). Next, we evaluated the FA composition of the analyzed families of phospholipids in purified myelin. Principal component analysis of myelin FAs revealed two separate clusters: the first includes control and STZ-GW3965-treated rats (red circle, **Fig. 2A**), the second the STZ diabetic animals (blue circle, Fig. 2A). Moreover, the correlation graph showed each FA analyzed associated to the two identified clusters (Fig. 2B). These plots and the myelin FA quantifications indicate that diabetes led to increased levels of saturated stearic (C18:0), behenic (C22:0), and lignoceric (C24:0) acids, whereas monounsaturated oleic acid (C18:1), nervonic acid (C22:1), and erucic (C24:1) acid decreased (Figs. 1C, 2A, B), indicating the inability of vehicle-treated diabetic rats to desaturate FAs. In addition, γ-linolenic acid (C18:3) was decreased in STZ rats, but arachidonic (C20:4), eicosapentaenoic (C20:5), and docosahexaenoic (C22:6) acids were increased (Figs. 1C, 2A, B). All changes in FA levels induced by diabetes were restored to normal levels by LXR activation (Figs. 1C, 2A, B). Furthermore, in diabetic animals, we detected a significant shift in the levels of monounsaturated FAs toward PUFAs (Fig. 1D), along with an increased ratio of C18:0/C18:1 corresponding to a decreased desaturation index (Fig. 1E, right part of the graph). In addition, diabetes also decreased the C18:1/C18:2 ratio, an index correlating with altered membrane fluidity (Fig. 1E, left part of the graph) (37). LXR activation once again brought the levels of these FAs to those of control rats and normalized both desaturation and membrane fluidity indexes (Fig. 1D, E). We also identified FA species such as C18:1 and C18:3 that are primarily associated with the most abundant glycosphingolipids (PC and GSL, Fig. 1A), as being less represented in the diabetic group relative to normal and diabetic GW3965-treated animals (Fig. 1F). Importantly, the lipid profile changes observed in diabetic rats were not detected in plasma,

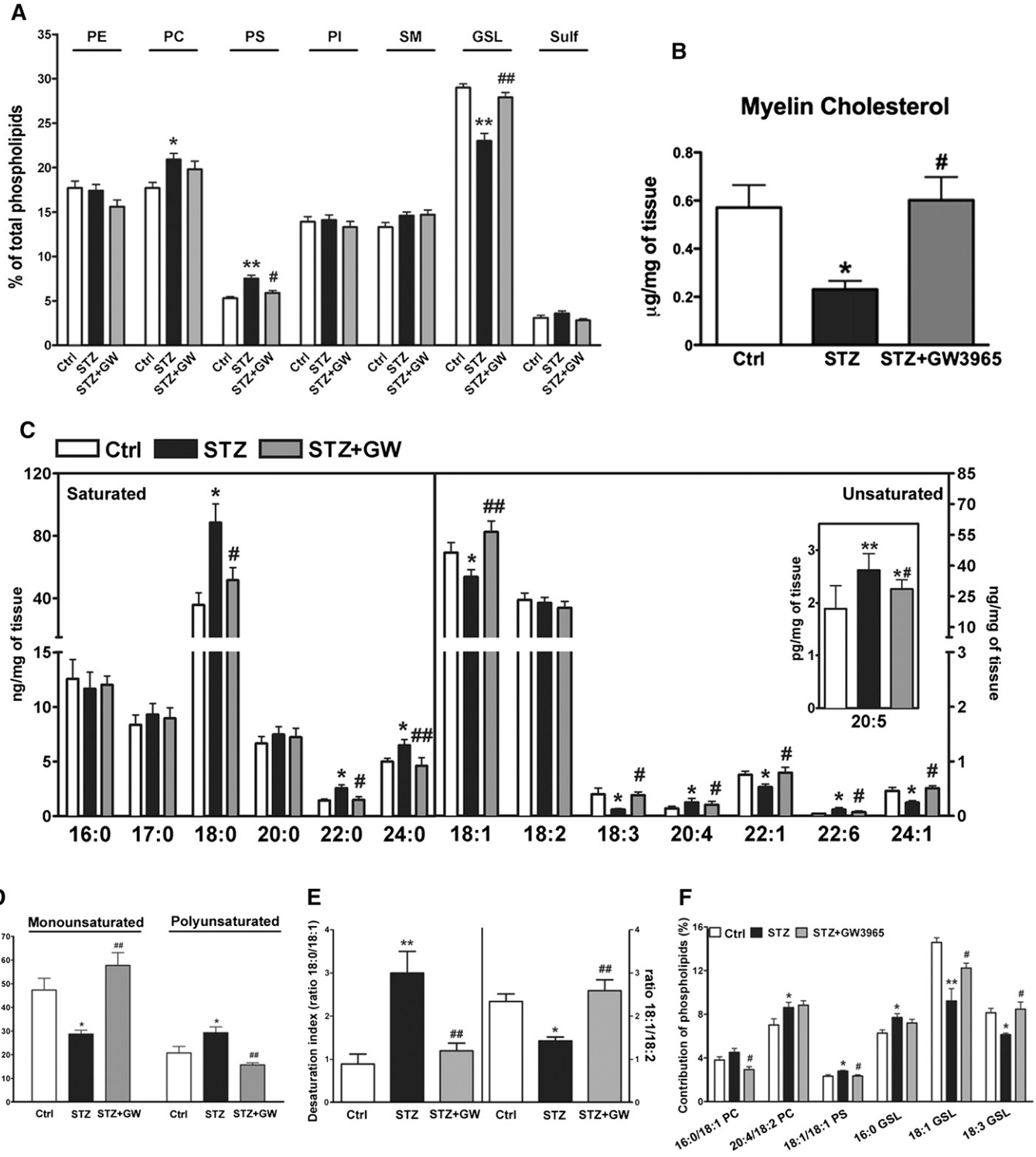

Fig. 1. Lipidomic profile of sciatic nerve purified myelin from control, STZ and STZ-treated with GW3965 animals. A: Percent of detected phospholipid families. B: Cholesterol levels. C: FA profile. D: Levels of monounsaturated and polyunsaturated FAs. E: Desaturation index as ratio of C18:0 (stearic acid)/C18:1 (oleic acid) and membrane fluidity as ratio of C18:1 (oleic acid)/C18:2 (linoleic acid). F: FAs associated to the significantly different phospholipids. Statistical analysis was performed by one-way ANOVA followed by Tukey-Kramer posttest. Data are expressed as mean ± SEM. n = 11 animals per group. $^{*}P < 0.05$, $^{**}P < 0.001$ vs. control rats; $^{\#}P < 0.05$, $^{\#\#}P < 0.001$ vs. STZ-treated rats. PE, phosphatidyl ethanolamine; PC, phosphatidyl coline; PS, phosphatidyl serine; PI, phosphatydil inositol; SM, sphingomyelin; GSL, glycosphingolipid; Sulf, sulfatide.

indicating that the effects of diabetes on lipogenesis occur locally in the sciatic nerve (data not shown). Taken together, these results indicate that myelin from diabetic animals has a different lipid composition pattern and that treatment with an LXR ligand, a lipogenic stimulus, restores the lipid profile to that of nondiabetic controls.

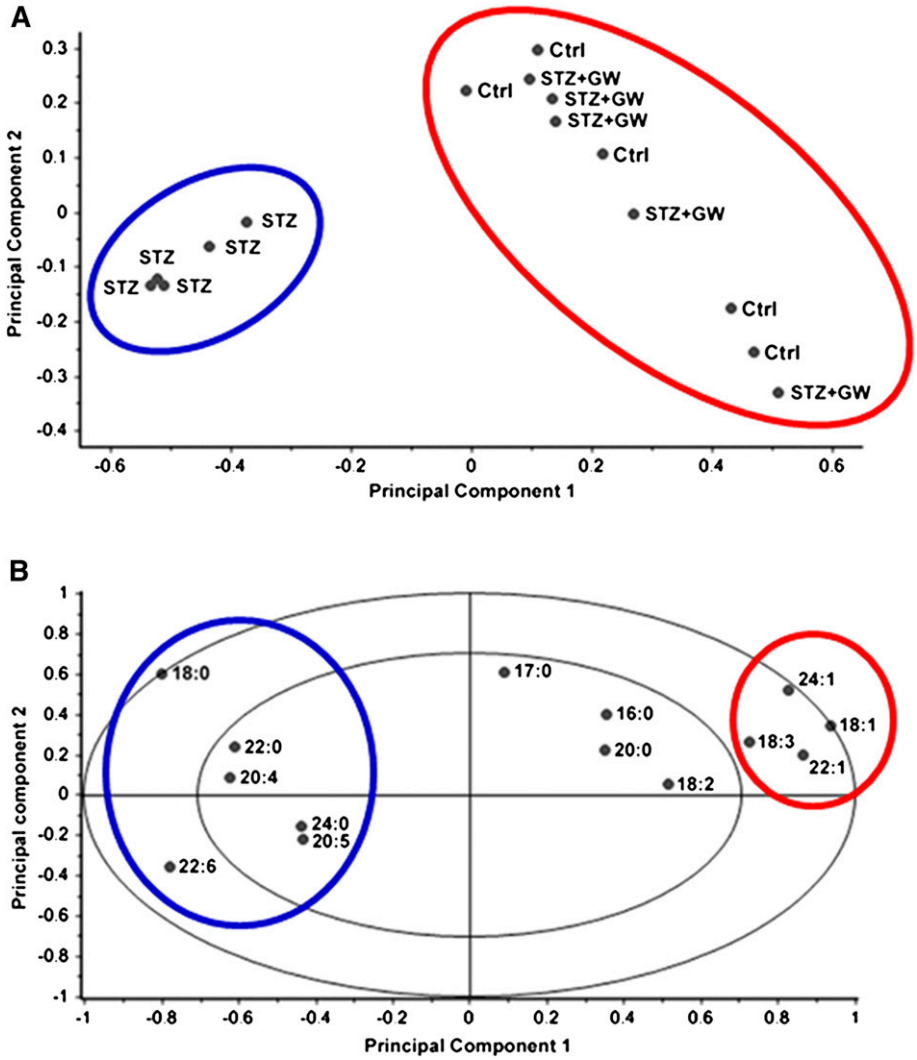

Fig. 2. Principal component analysis of sciatic nerve purified myelin from control, STZ, and STZ-treated with GW3965 animals. A: Score plot of the lipid composition analysis of five animals per group. The two coordinates (Principal Component 1 and Principal Component 2) represent together >80% of the variance of these 15 samples. Principal Component 1 accounts for 73% of this variance and clearly identifies two clusters. The first includes the control and STZ-GW3965 animals (red circle), whereas the diabetic rats (blue circle) belong to the second cluster, indicating that the lipid profile is different between the two clusters. B: Correlation loadings plot computed for each FA analyzed for the displayed principal components. The red circle (control and STZGW3965-treated groups) and the blue circle (STZ-vehicle treated group) represent the FAs enriched in the considered cluster. For instance, 18:0 may be considered a marker for the STZ group, whereas 18:1 is a marker for control and STZ-GW3965-treated animals. The two ellipses indicate how much variance is taken into account. The outer ellipse accounts for 100% of explained variance. The inner ellipse shows 50% of explained variance.

LXR activation restores expression of key genes in FA biosynthesis suppressed by diabetes

To better understand the observed changes in myelin lipid profiles, the mRNA level of genes involved in lipid biosynthesis were analyzed in the sciatic nerve of control, STZ, and STZ-GW3965-treated rats. We found that lipogenic genes such as SREBF-1c, acetyl-CoA carboxylase α (ACACA), FAS, SCD-1, and -2 [SCD-2, the main isoform expressed in peripheral nerves (38)], and FA desaturase-1 and -2, were all downregulated in diabetic sciatic nerve, and that their expression was brought back to nondiabetic levels by pharmacologic LXR activation (**Fig. 3**). Expression of enzymes involved in FA elongation, such as elongase of very long chain FAs 5 and 6 , were unchanged in all experimental groups (Fig. 3). As expected, nondiabetic rats treated with GW3965 also showed increased expression of SREBF-1c, FAS, and SCD-1 and -2 compared with nondiabetic rats receiving vehicle (see supplementary Fig. I). However, in this nonpathological setting, these changes in gene expression are not sufficient to significantly affect myelin lipid composition (see supplementary Fig. II). These findings show that pharmacological LXR activation can restore the levels of key genes involved in lipid synthesis whose expression is suppressed in the sciatic nerve of diabetic animals.

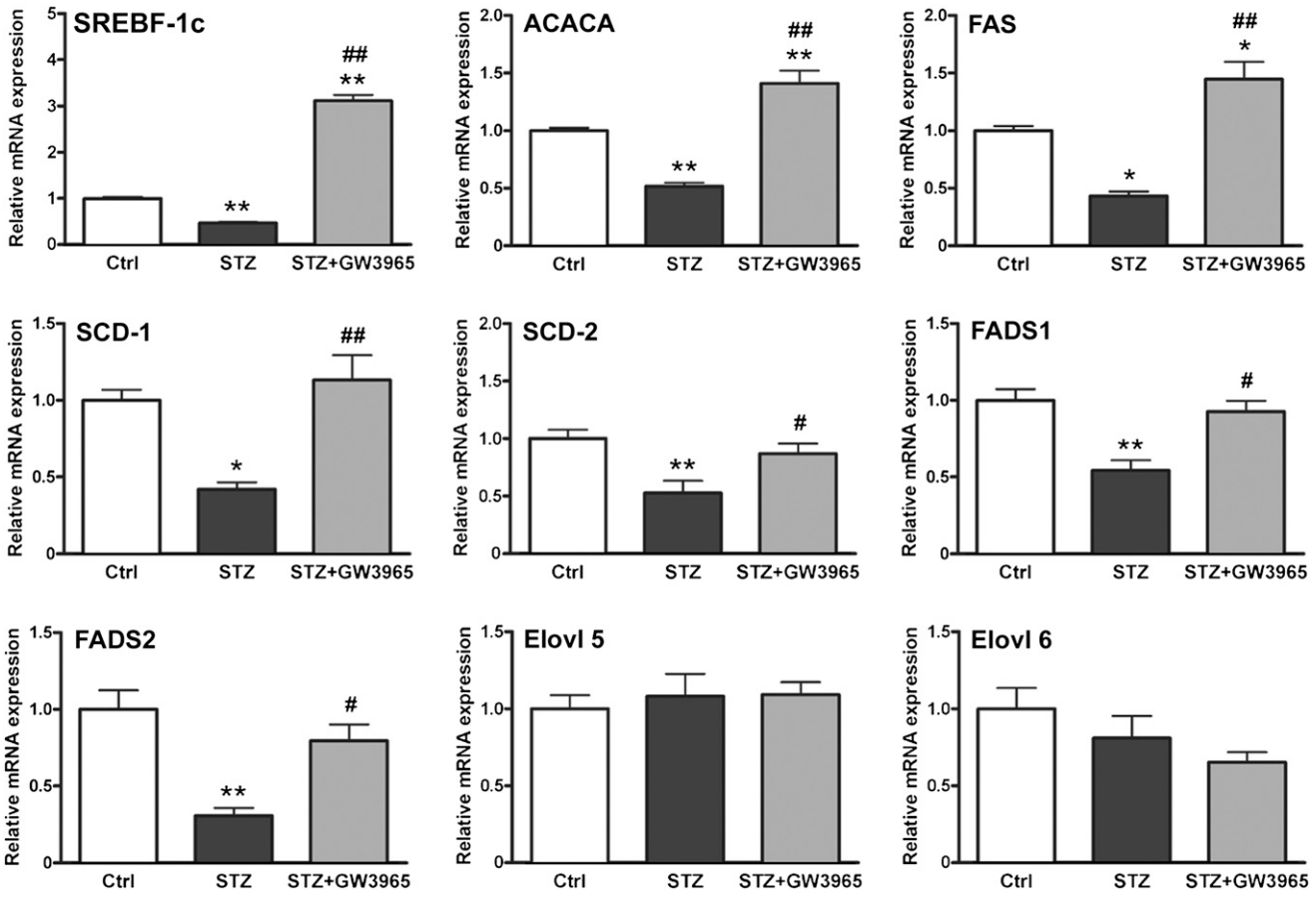

Fig. 3. Expression profile of FA biosynthesis genes. Statistical analysis was performed by one-way ANOVA followed by Tukey-Kramer posttest. Data are expressed as mean ± SEM. n = 8 animals per group. $^{*}P < 0.05$, $^{**}P < 0.001$ vs. control rats; $^{\#}P < 0.05$, $^{\#\#}P < 0.001$ vs. STZ-treated rats.

Activation of LXR restores transcriptionally active SREBF-1c

Because SREBF-1c is a classic LXR target gene and all FA biosynthesis genes affected by diabetes are known to be regulated by this lipogenic transcription factor (39), we measured the levels of the cytoplasmic precursor and the mature nuclear form of SREBF-1c. The precursor form of SREBF-1c is anchored in endoplasmic reticulum membranes. Upon stimulation (e.g., insulin, in the case of SREBF-1c), the precursor is cleaved into a mature form that shuttles to the nucleus to activate expression of enzymes involved in FA biosynthesis (40).

We found that the sciatic nerve of diabetic animals contains less transcriptionally active SREBF-1 (mature form), a decrease that is rescued by LXR activation (**Fig. 4A**). The SREBF-1 antibody used was validated using extracts from HEK293T cells transfected with Flag-tagged expression constructs for the mature forms of SREBF-1a (41), SREBF-1c (41), and SREBF-2 (42). The SREBF-1 antibody detected the mature forms of SREBF-1a and SREBF-1c, but it did not cross-react with SREBF-2 (see supplementary Fig. III). To exclude a role for SREBF-1a, we measured the mRNA levels of this transcription factor. Expression of SREBF-1a was not affected by diabetes or treatment with the LXR agonist GW3965 (see supplementary Fig. IV). These results indicate that SREBF-1c is the isoform most affected by DPN.

To substantiate these findings, we performed colocalization experiments between SREBF-1c and nuclei using immunofluorescence. We drew a region of interest to precisely outline nuclei and assess the presence of transcriptionally active SREBF-1c. SREBF-1c (green) and nuclei (blue) highly colocalized in the sciatic nerve of control and diabetic rats treated with GW3965 (Fig. 4B, C). In contrast, only a partial colocalization was observed in the sciatic nerve of STZ vehicle-treated animals (Fig. 4B, C). These results suggest that diabetes reduces the transcriptionally active form of the lipogenic transcription factor SREBF-1c in the sciatic nerve, and that its levels are normalized upon LXR activation.

LXR activation improves myelin protein composition

In addition to lipid, myelin contains about 20–30% protein. We found that the levels of P0 protein, which represent between 50% and 70% of total myelin protein in peripheral nerves (14), were decreased by diabetes (**Fig. 5**), confirming data already present in the literature (24, 43). Pharmacological LXR activation restored P0 levels to those found in nondiabetic control rats; levels of PMP22 were unchanged among experimental groups (Fig. 5).

The sciatic nerve of STZ-treated diabetic rats shows myelin abnormalities that can be reversed by LXR activation

To investigate whether the observed effects on myelin lipid and protein composition induced by diabetes are

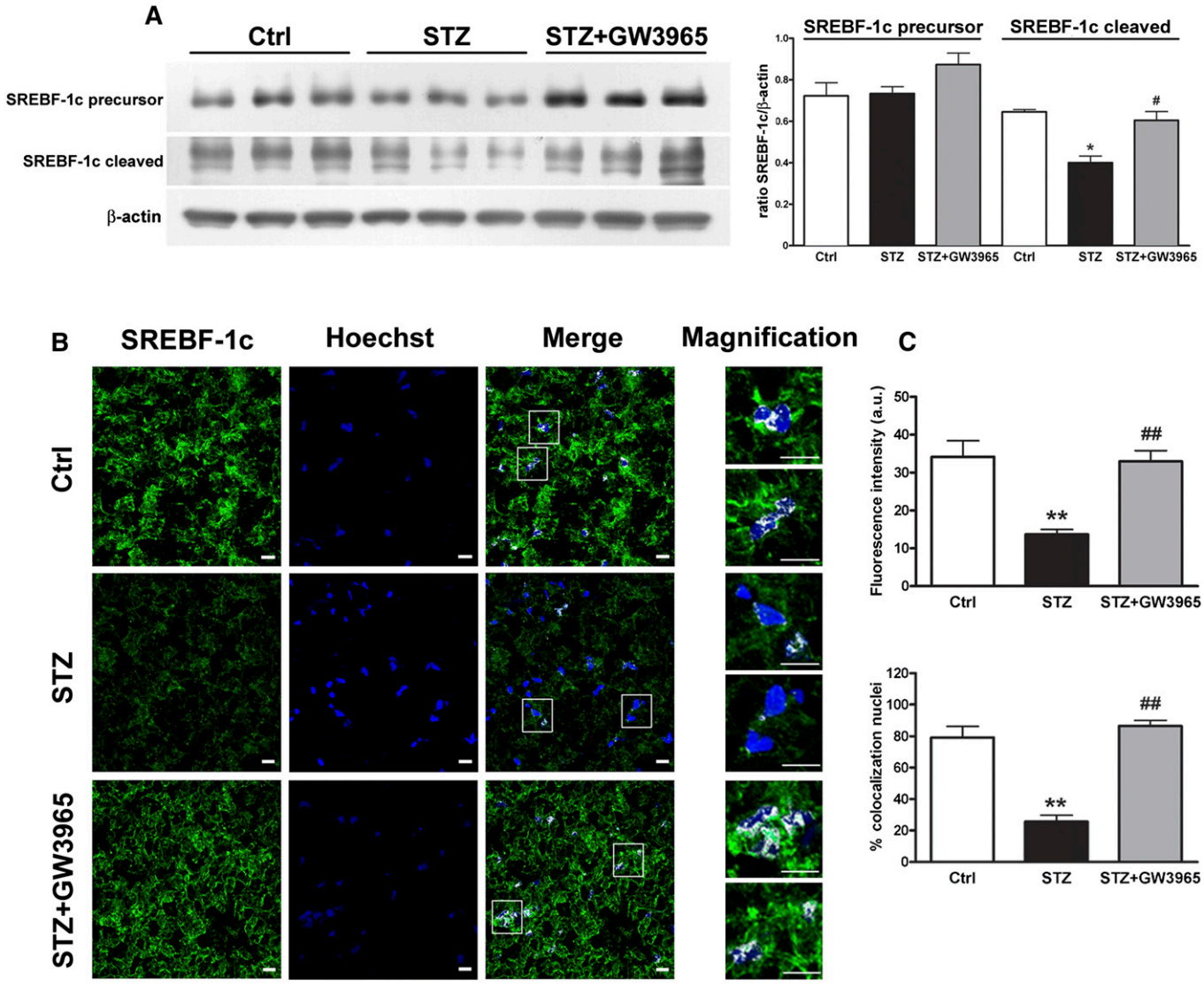

Fig. 4. LXR activation restored the transcriptionally active form of the lipogenic transcription factor SREBF-1c that is blunted in diabetic rats. A: Representative Western blot analysis and quantification of SREBF-1c precursor (125 kDa) and transcriptionally active form (cleaved, 68 kDa) in control, STZ, and STZ-treated with GW3965 rat sciatic nerve. B: Fluorescence images of control, STZ, and STZ-treated with GW3965 rat sciatic nerves. SREBF-1c (green) and nuclei (blue) are highly colocalized (white spots in merge images) in sciatic nerve of control rats and diabetic animals receiving GW3965. In contrast, only a partial colocalization was observed in sciatic nerve of STZ rats. To better appreciate nuclear SREBF-1c localization, some highlighted nuclei are magnified (white squares). Scale bars: 10 μm. C: Quantitative analysis of SREBF-1 protein within the nuclei of control, STZ, and STZ-treated with GW3965 rat sciatic nerves. Upper panel: fluorescence associated to positive nuclei. Lower panel: colocalization percent of SREBF-1 with nuclei. Statistical analysis was performed by one-way ANOVA followed by Tukey-Kramer posttest. Data are expressed as mean ± SEM. n = 3 animals per group. $^{*}P<0.05$, $^{**}P< 0.001$ versus control rats; $^{\#}P< 0.05$, $^{\#\#}P< 0.001$ versus STZ-treated rats.

associated with myelin abnormalities, we performed morphometric and morphological analyses. We observed that myelin fibers from diabetic animals have a reduction in normal fibers and show increased myelin abnormalities (**Fig. 6A, B**). These pathological changes were reversed to what is seen in nondiabetic animals by treatment with the LXR ligand (Fig. 6A, B). In particular, the diabetic state increased myelin infoldings, and these were restored to normal levels by LXR ligand treatment (Fig. 6C). Percentage of alterations in myelin compaction and irregular fiber shape (Fig. 6D, E), as well as *g* ratio and axonal diameter (Fig. 6F, G), were similar among experimental groups. Myelin ultrastructure studies using transmission electron microscopy (TEM) confirmed observations from myelin fiber analysis (Fig. 6H). These data show that STZ-induced peripheral neuropathy is characterized by myelin abnormalities such as infoldings, which are reversed to normal by activation of LXR.

DISCUSSION

Alterations of myelin lipid and protein composition in peripheral nerves are often associated with metabolic derangements and neurodegenerative disorders, and can result in reduced saltatory conduction of nerve impulses throughout the axons (37). Peripheral neuropathy is a

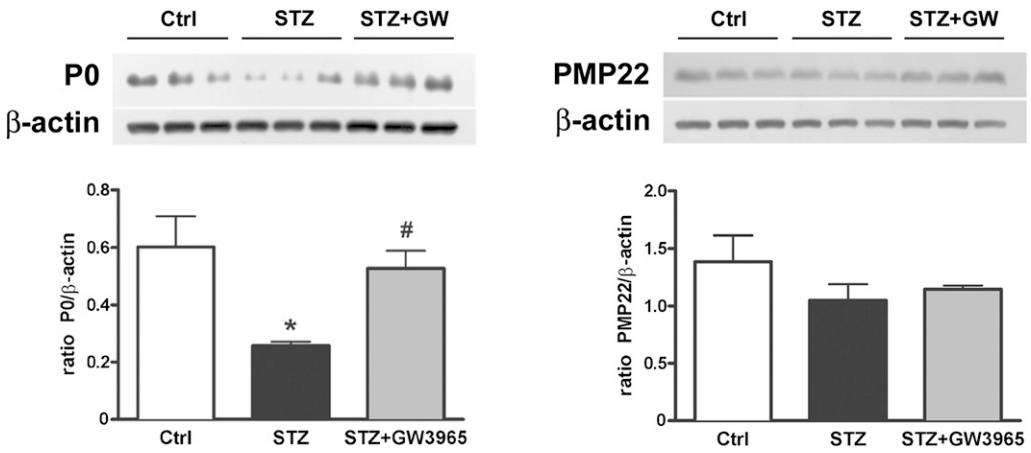

Fig. 5. Myelin protein analysis. Representative P0 and PMP22 Western blot analyses and relative quantifications. Statistical analysis was performed by one-way ANOVA followed by Tukey-Kramer posttest. Data are expressed as mean ± SEM. n = 3 animals per group. $^{*}P < 0.05$ vs. control rats; $^{\#}P < 0.05$ vs. STZ-treated rats.

complication of diabetes that comprises functional and structural changes in peripheral nerves, such as a reduction in nerve conduction velocity, axonal degeneration, paranodal demyelination, and loss of myelinated fibers (4, 5). Some of the morphological alterations in myelinated fibers of peripheral nerves associated with hyperglycemia are also seen in rat models of STZ-induced diabetic neuropathy (13). These alterations include myelin invaginations in the axoplasm (infoldings) and myelin evaginations in the Schwann cell cytoplasm (outfoldings), as well as alterations in myelin compaction such as abnormally wide incisures and aberrant separation of myelin lamellae. Similar to those seen in aged rodents (44), the predominant myelin abnormalities found in STZ-treated rats are myelin infoldings (13).

In the present study, we tested the following hypotheses: *i*) diabetes affects myelin lipid composition, and such changes may be associated with myelin abnormalities, and *ii*) pharmacologic activation of the LXR nuclear receptor may restore myelin composition and reverse diabetes-induced alterations in myelin. We have found that diabetes indeed induces an altered lipid profile in myelin. Diabetes results in a concomitant decrease in myelin of cholesterol and monounsaturated FAs, and an increase in polyunsaturated FAs, which together with changes in phospholipid species and in the desaturation (C18:0/C18:1 ratio) and membrane fluidity (C18:1/C18:2 ratio) indexes, may be responsible for altered myelin lipid-protein interactions. We also observed in the hyperglycemic state a reduction in myelin P0. It appears that diabetes modifies myelin's lipid profile and protein composition, changes that result in altered membrane fluidity and myelin abnormalities (21, 45). These data are consistent with work showing that changes in myelin lipid composition in STZ-treated animals correlate with altered biophysical properties of the myelin sheath, as assessed by electron spin resonance spectroscopy (22). Our principal component analysis shows that control and diabetic rats differ in the lipid composition of myelin. The differences may be the result of decreased expression of genes involved in FA biosynthesis, as most of them are downregulated by DPN. Furthermore, these changes were associated with increased myelin abnormalities and reduced performance of diabetic animals in functional tests. While STZ-diabetic animals show profound differences in body weight and nutritional status compared with control rats, plasma lipids do not show the altered profile seen in myelin lipids, suggesting that DPN has a specific impact on peripheral nerve lipid synthesis.

Because insulin is a known activator of SREBF-1c transcription, the lack of insulin in STZ-treated rats may account for the observed reduction of nuclear, active SREBF-1c (46). It has been reported that insulin activates SREBF-1c and FAS promoter activity directly in rat-isolated Schwann cells, indicating that this hormone regulates lipid metabolism in peripheral nerves (20). The role of this regulatory pathway in peripheral nerves is still unclear; nevertheless, its downregulation contributes to the pathogenesis of DPN. Thus, it may be possible that insulin administration, by activating SREBF-1c and FA synthesis, could ameliorate the altered myelin lipid and protein pattern induced by diabetes. The response to insulin requires two LXR binding sites in the promoter of SREBF-1c; disruption of these LXR binding sites does not lower basal transcription but severely reduces the transcriptional induction induced by insulin (46). In our diabetic model, to reactivate SREBF-1c, we decided to use a selective LXR ligand rather than insulin itself because in addition to its ability to induce SREBF-1c expression, insulin can also reduce systemic glucose levels, and thus obscure the specific effects due to exclusive activation of SREBF-1c. LXR activation in diabetic rats restored expression of key genes of FAS synthesis and brought myelin lipid content back to control levels. These beneficial effects of LXR activation are probably due to LXR's ability to restore the levels of nuclear-active SREBF-1c. Treatment with synthetic LXR ligands also brought back to normal the levels of myelin P0. Whether this is due to SREBF-1c activation or to changes in myelin lipid content that influence protein packaging in this membrane remains an open question.

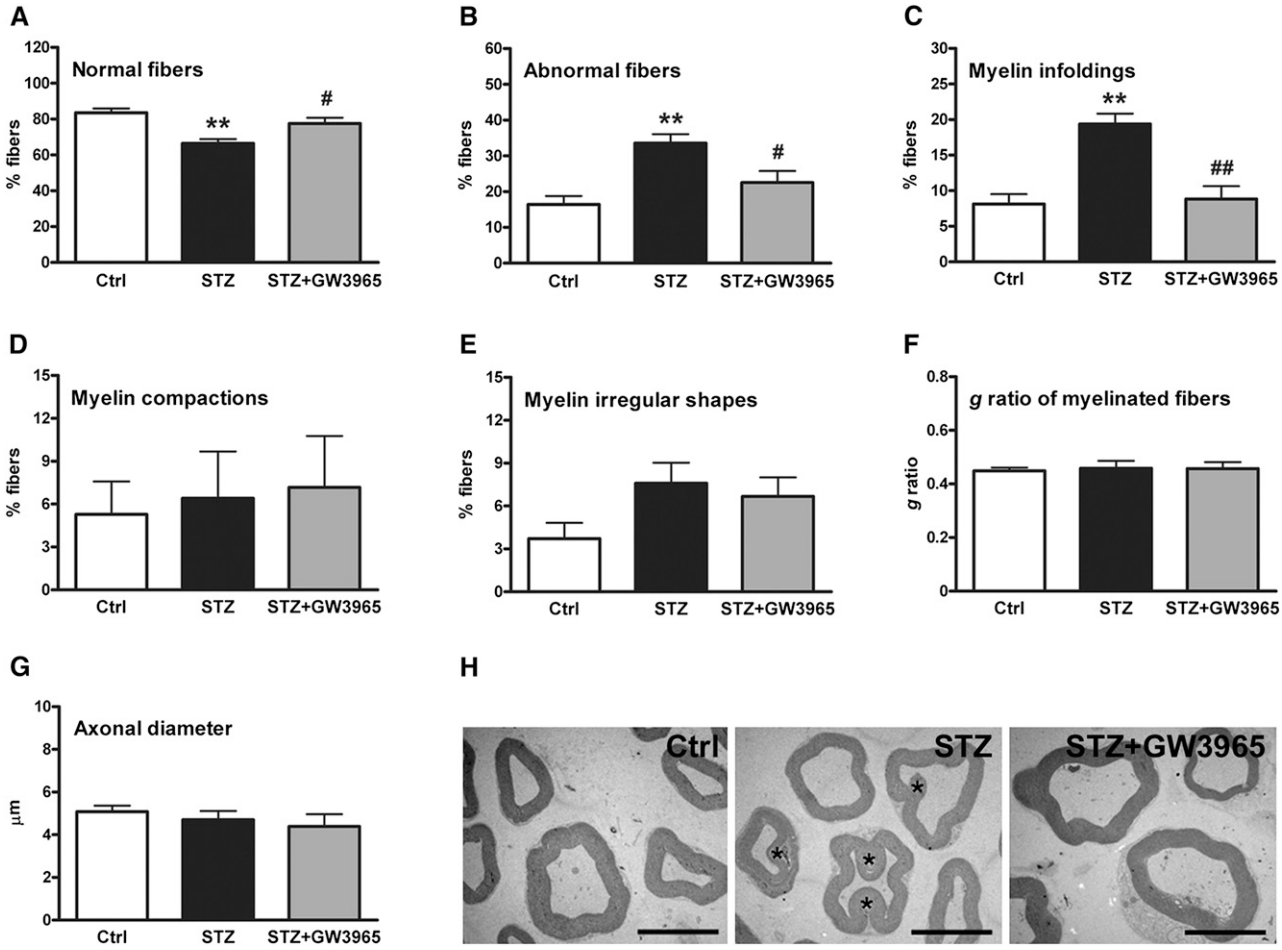

Fig. 6. Morphometric and TEM analysis of myelinated fibers in sciatic nerve of control, STZ, and STZ-treated with GW3965 rats. A: Percentage of normal fibers. B: Percentage of abnormal fibers. C: Percentage of fibers with myelin infoldings. D: Percentage of fibers with alterations in myelin compaction. E: Percentage of fibers with myelin irregular shapes. F: *g* ratio of myelinated fibers. G: Axonal diameter. H: Detail of myelinated nerves analyzed by TEM. Myelin infoldings are observed in diabetic rats (asterisks). Scale bars: 8 μm. Statistical analysis was performed by one-way ANOVA followed by Tukey-Kramer posttest. Data are expressed as mean ± SEM. n = 8 animals per group. $^{**}P < 0.001$ vs. control rats; $^{\#}P < 0.05$ and $^{\#\#}P < 0.001$ vs. STZ-treated rats.

Because neuroactive steroids enhance P0 expression (47), and LXR activation also increases neuroactive steroid levels in sciatic nerve, it is possible that the beneficial effects of LXR activation on P0 levels are due to greater concentration of neurosteroids (24). LXR activation also restored myelin structure to that seen in nondiabetic rats and improved performance of treated animals in functional tests. These improvements were seen in the absence of side effects that have been associated with LXR-SREBF-1c activation, such as hepatic steatosis (data not shown). This is probably the result of our very mild, but effective, dosing regimen. It is interesting to note that LXR double knockout mice exhibit thinner myelin sheaths in peripheral nerves (48). Together with our present and past findings (24), these observations highlight the significance of the LXR-SREBF-1c axis in the control of myelin lipid content, and suggest that synthetic LXR activators may be useful to reverse myelin abnormalities brought about by diabetes.

Studies on diabetic neuropathy are largely concentrated on the axon, as it seems that axonal defects may be primarily responsible for neuropathic symptoms (49). However, studies on diabetic subjects reveal that demyelination occurs before axonal loss (8, 9). Moreover, myelin abnormalities associated with type 1 diabetes correlate with reductions in nerve conduction velocity (6). Because activation of LXR with synthetic ligands tackles specific myelin alterations and neuroactive steroids, our findings hint that LXR activators may have potential for the treatment of DPN.

The authors thank Drs. Silvia Giatti, Marzia Pesaresi, Donato Calabrese, and Roberto Bianchi for their valuable help in animal handling, and Flavio Giavarini for GC-MS analyses. We also thank Dr. Monica Beltrame for helpful comments on the manuscript and Elda Desiderio Pinto for administrative assistance.

REFERENCES

1. ADA. 2007. Standards of medical care in diabetes–2007. *Diabetes Care.* **30 (Suppl.):** 4–41.
2. Gordois, A., P. Scuffham, A. Shearer, A. Oglesby, and J. A. Tobian. 2003. The health care costs of diabetic peripheral neuropathy in the US. *Diabetes Care.* **26:** 1790–1795.
3. Herman, W. H. 2007. Diabetes epidemiology: guiding clinical and public health practice: the Kelly West Award Lecture, 2006. *Diabetes Care.* **30:** 1912–1919.

4. Sugimoto, K., Y. Murakawa, and A. A. Sima. 2000. Diabetic neuropathy–a continuing enigma. *Diabetes Metab. Res. Rev.* **16:** 408–433.
5. Vinik, A. I., T. S. Park, K. B. Stansberry, and G. L. Pittenger. 2000. Diabetic neuropathies. *Diabetologia.* **43:** 957–973.
6. Sima, A. A., and T. Brismar. 1985. Reversible diabetic nerve dysfunction: structural correlates to electrophysiological abnormalities. *Ann. Neurol.* **18:** 21–29.
7. Eckersley, L. 2002. Role of the Schwann cell in diabetic neuropathy. *Int. Rev. Neurobiol.* **50:** 293–321.
8. Malik, R. A., S. Tesfaye, P. G. Newrick, D. Walker, S. M. Rajbhandari, I. Siddique, A. K. Sharma, A. J. Boulton, R. H. King, P. K. Thomas, et al. 2005. Sural nerve pathology in diabetic patients with minimal but progressive neuropathy. *Diabetologia.* **48:** 578–585.
9. Valls-Canals, J., M. Povedano, J. Montero, and J. Pradas. 2002. Diabetic polyneuropathy. Axonal or demyelinating? *Electromyogr. Clin. Neurophysiol.* **42:** 3–6.
10. Yagihashi, S. 1997. Nerve structural defects in diabetic neuropathy: do animals exhibit similar changes? *Neurosci. Res. Commun.* **21:** 25–32.
11. Biessels, G. J., N. A. Cristino, G. J. Rutten, F. P. Hamers, D. W. Erkelens, and W. H. Gispen. 1999. Neurophysiological changes in the central and peripheral nervous system of streptozotocin-diabetic rats. Course of development and effects of insulin treatment. *Brain.* **122:** 757–768.
12. Dyck, P. J., B. R. Zimmerman, T. H. Vilen, S. R. Minnerath, J. L. Karnes, J. K. Yao, and J. F. Poduslo. 1988. Nerve glucose, fructose, sorbitol, myo-inositol, and fiber degeneration and regeneration in diabetic neuropathy. *N. Engl. J. Med.* **319:** 542–548.
13. Veiga, S., E. Leonelli, M. Beelke, L. M. Garcia-Segura, and R. C. Melcangi. 2006. Neuroactive steroids prevent peripheral myelin alterations induced by diabetes. *Neurosci. Lett.* **402:** 150–153.
14. Garbay, B., A. M. Heape, F. Sargueil, and C. Cassagne. 2000. Myelin synthesis in the peripheral nervous system. *Prog. Neurobiol.* **61:** 267–304.
15. Waxman, S. G., and J. M. Ritchie. 1993. Molecular dissection of the myelinated axon. *Ann. Neurol.* **33:** 121–136.
16. Norton, W. T., and S. E. Poduslo. 1973. Myelination in rat brain: changes in myelin composition during brain maturation. *J. Neurochem.* **21:** 759–773.
17. Norton, W. T., and S. E. Poduslo. 1973. Myelination in rat brain: method of myelin isolation. *J. Neurochem.* **21:** 749–757.
18. Detering, N. K., and M. A. Wells. 1976. The non-synchronous synthesis of myelin components during early stages of myelination in the rat optic nerve. *J. Neurochem.* **26:** 253–257.
19. Nussbaum, J. L., N. Neskovic, and P. Mandel. 1969. A study of lipid components in brain of the 'Jimpy' mouse, a mutant with myelin deficiency. *J. Neurochem.* **16:** 927–934.
20. de Preux, A. S., K. Goosen, W. Zhang, A. A. Sima, H. Shimano, D. M. Ouwens, M. Diamant, J. L. Hillebrands, J. Rozing, G. Lemke, et al. 2007. SREBP-1c expression in Schwann cells is affected by diabetes and nutritional status. *Mol. Cell. Neurosci.* **35:** 525–534.
21. Verheijen, M. H., N. Camargo, V. Verdier, K. Nadra, A. S. de Preux Charles, J. J. Medard, A. Luoma, M. Crowther, H. Inouye, H. Shimano, et al. 2009. SCAP is required for timely and proper myelin membrane synthesis. *Proc. Natl. Acad. Sci. USA.* **106:** 21383–21388.
22. Zuvic-Butorac, M., J. Kriz, A. Simonic, and M. Schara. 2001. Fluidity of the myelin sheath in the peripheral nerves of diabetic rats. *Biochim. Biophys. Acta.* **1537:** 110–116.
23. Coste, T. C., A. Gerbi, P. Vague, J. M. Maixent, G. Pieroni, and D. Raccah. 2004. Peripheral diabetic neuropathy and polyunsaturated fatty acid supplementations: natural sources or biotechnological needs? *Cell. Mol. Biol. (Noisy-le-grand).* **50:** 845–853.
24. Cermenati, G., S. Giatti, G. Cavaletti, R. Bianchi, O. Maschi, M. Pesaresi, F. Abbiati, A. Volonterio, E. Saez, D. Caruso, et al. 2010. Activation of the liver X receptor increases neuroactive steroid levels and protects from diabetes-induced peripheral neuropathy. *J. Neurosci.* **30:** 11896–11901.
25. Caruso, D., S. Scurati, O. Maschi, L. De Angelis, I. Roglio, S. Giatti, L. M. Garcia-Segura, and R. C. Melcangi. 2008. Evaluation of neuroactive steroid levels by liquid chromatography-tandem mass spectrometry in central and peripheral nervous system: effect of diabetes. *Neurochem. Int.* **52:** 560–568.
26. Pesaresi, M., O. Maschi, S. Giatti, L. M. Garcia-Segura, D. Caruso, and R. C. Melcangi. 2010. Sex differences in neuroactive steroid levels in the nervous system of diabetic and non-diabetic rats. *Horm. Behav.* **57:** 46–55.
27. Roglio, I., S. Giatti, M. Pesaresi, R. Bianchi, G. Cavaletti, G. Lauria, L. M. Garcia-Segura, and R. C. Melcangi. 2008. Neuroactive steroids and peripheral neuropathy. *Brain Res. Rev.* **57:** 460–469.
28. Leonelli, E., R. Bianchi, G. Cavaletti, D. Caruso, D. Crippa, L. M. Garcia-Segura, G. Lauria, V. Magnaghi, I. Roglio, and R. C. Melcangi. 2007. Progesterone and its derivatives are neuroprotective agents in experimental diabetic neuropathy: a multimodal analysis. *Neuroscience.* **144:** 1293–1304.
29. Kalaany, N. Y., and D. J. Mangelsdorf. 2006. LXRS and FXR: the yin and yang of cholesterol and fat metabolism. *Annu. Rev. Physiol.* **68:** 159–191.
30. Schultz, J. R., H. Tu, A. Luk, J. J. Repa, J. C. Medina, L. Li, S. Schwendner, S. Wang, M. Thoolen, D. J. Mangelsdorf, et al. 2000. Role of LXRs in control of lipogenesis. *Genes Dev.* **14:** 2831–2838.
31. Melcangi, R. C., F. Celotti, P. Castano, and L. Martini. 1992. Is the 5 alpha-reductase-3 alpha-hydroxysteroid dehydrogenase complex associated with the myelin in the peripheral nervous system of young and old male rats? *Endocr. Regul.* **26:** 119–125.
32. Taguchi, R., and M. Ishikawa. 2010. Precise and global identification of phospholipid molecular species by an Orbitrap mass spectrometer and automated search engine Lipid Search. *J. Chromatogr. A.* **1217:** 4229–4239.
33. Mayhew, T. M., and A. K. Sharma. 1984. Sampling schemes for estimating nerve fibre size. I. Methods for nerve trunks of mixed fascicularity. *J. Anat.* **139:** 45–58.
34. Mayhew, T. M., and A. K. Sharma. 1984. Sampling schemes for estimating nerve fibre size. II. Methods for unifascicular nerve trunks. *J. Anat.* **139:** 59–66.
35. Arbuthnott, E. R., I. A. Boyd, and K. U. Kalu. 1980. Ultrastructural dimensions of myelinated peripheral nerve fibres in the cat and their relation to conduction velocity. *J. Physiol.* **308:** 125–157.
36. Arbuthnott, E. R., K. J. Ballard, I. A. Boyd, and K. U. Kalu. 1980. Quantitative study of the non-circularity of myelinated peripheral nerve fibres in the cat. *J. Physiol.* **308:** 99–123.
37. Chrast, R., G. Saher, K. A. Nave, and M. H. Verheijen. 2011. Lipid metabolism in myelinating glial cells: lessons from human inherited disorders and mouse models. *J. Lipid Res.* **52:** 419–434.
38. Garbay, B., F. Boiron-Sargueil, M. Shy, T. Chbihi, H. Jiang, J. Kamholz, and C. Cassagne. 1998. Regulation of oleoyl-CoA synthesis in the peripheral nervous system: demonstration of a link with myelin synthesis. *J. Neurochem.* **71:** 1719–1726.
39. Shimomura, I., Y. Bashmakov, and J. D. Horton. 1999. Increased levels of nuclear SREBP-1c associated with fatty livers in two mouse models of diabetes mellitus. *J. Biol. Chem.* **274:** 30028–30032.
40. Wang, X., R. Sato, M. S. Brown, X. Hua, and J. L. Goldstein. 1994. SREBP-1, a membrane-bound transcription factor released by sterol-regulated proteolysis. *Cell.* **77:** 53–62.
41. Toth, J. I., S. Datta, J. N. Athanikar, L. P. Freedman, and T. F. Osborne. 2004. Selective coactivator interactions in gene activation by SREBP-1a and -1c. *Mol. Cell. Biol.* **24:** 8288–8300.
42. Jeon, T. I., B. Zhu, J. L. Larson, and T. F. Osborne. 2008. SREBP-2 regulates gut peptide secretion through intestinal bitter taste receptor signaling in mice. *J. Clin. Invest.* **118:** 3693–3700.
43. Kawashima, R., H. Kojima, K. Nakamura, A. Arahata, Y. Fujita, Y. Tokuyama, T. Saito, S. Furudate, T. Kurihara, S. Yagishita, et al. 2007. Alterations in mRNA expression of myelin proteins in the sciatic nerves and brains of streptozotocin-induced diabetic rats. *Neurochem. Res.* **32:** 1002–1010.
44. Azcoitia, I., E. Leonelli, V. Magnaghi, S. Veiga, L. M. Garcia-Segura, and R. C. Melcangi. 2003. Progesterone and its derivatives dihydroprogesterone and tetrahydroprogesterone reduce myelin fiber morphological abnormalities and myelin fiber loss in the sciatic nerve of aged rats. *Neurobiol. Aging.* **24:** 853–860.
45. Lee, A. G. 2003. Lipid-protein interactions in biological membranes: a structural perspective. *Biochim. Biophys. Acta.* **1612:** 1–40.
46. Chen, G., G. Liang, J. Ou, J. L. Goldstein, and M. S. Brown. 2004. Central role for liver X receptor in insulin-mediated activation of Srebp-1c transcription and stimulation of fatty acid synthesis in liver. *Proc. Natl. Acad. Sci. USA.* **101:** 11245–11250.
47. Melcangi, R. C., I. T. Cavarretta, M. Ballabio, E. Leonelli, A. Schenone, I. Azcoitia, L. Miguel Garcia-Segura, and V. Magnaghi. 2005. Peripheral nerves: a target for the action of neuroactive steroids. *Brain Res. Brain Res. Rev.* **48:** 328–338.
48. Makoukji, J., G. Shackleford, D. Meffre, J. Grenier, P. Liere, J. M. Lobaccaro, M. Schumacher, and C. Massaad. 2011. Interplay between LXR and Wnt/{beta}-catenin signaling in the negative regulation of peripheral myelin genes by oxysterols. *J. Neurosci.* **31:** 9620–9629.
49. Krarup, C. 2003. An update on electrophysiological studies in neuropathy. *Curr. Opin. Neurol.* **16:** 603–612.